ISSN 2176-5480

22nd International Congress of Mechanical Engineering (COBEM 2013)
November 3-7, 2013, Ribeirão Preto, SP, Brazil

STRESS ANALYSIS OF A RIVER CURRENT HYDROKINETIC TURBINE BLADE

Dalmo Inácio Galdez Costa
Flaminio Levy Neto
Marcus Vinícius Girão de Morais
Guilherme Vaz Ferreira
Matheus B. A. M. Oberg
Jonatas Teófilo Louzada da Cunha
Universidade de Brasília, UnB-FT-ENM, 70910-900, Brasília, DF, Brasil
dalmodj@gmail.com, flaminio@unb.br, mumorais@gmail.com, guilhermedf@gmail.com, matheus.oberg@gmail.com, jonatasdf@gmail.com

Abstract. *In view of the exhaustion of fossil fuels, predicted to take place in a very near future, and the severe environmental as well as health problems associated with the burning of oil, renewable and clean sources of energy are being developed and gaining increased attention worldwide. Hydrokinetic submerged river current turbines are an attractive option in this scenario, due to their predictability and high energy density. This work is mainly concerned with the development of a three blades, horizontal axis, 500kW river current hydrokinetic turbine, planned to be installed downstream to Tucuruí Dam in Brazil. These turbines are installed in narrow and deep river straits, where the flow of water is both faster and more uniform. Their blades can be manufactured using aluminum alloy or stainless steel. Using the finite element (FE) program ANSYS, stress analysis of 4.5m long aluminum, AA 6061-T6, and stainless steel, AISI 304, blades will be presented.*
In service, the blades are subjected to a distributed hydrodynamic load, along the radial direction, with normal and tangential components. The resultant force on each blade is W = 55.3 kN (5637 Kgf). The blades were modeled as a cantilever beam, initially solid, using a 3-D FE mesh. According to the static simulations carried out so far: (i) the resultant force of the hydrodynamic load is greater than the self weight of the solid Al blade (2567Kgf) and lower than the weight of solid steel blade (7630 Kgf); (ii) the maximum equivalent Von Mises stress (close to the clamped root) is less than 40 % of the yield stress of the alloys, in the worst case (hollow shell type steel blade); and (iii) the maximum tensile stress reached about 70% of the fatigue limit stress of the aluminum 6061-T6, in the worst case (hollow shell type Al blade). Thus, since the safety factor for fatigue failure is less than 1/3, the next step of the work is the optimization of the design. In particular, to reinforce the blades in the region close to the clamped root.

Keywords: *Metallic hydrokinetic turbine blades, stress analysis.*

1. INTRODUCTION

From the early 1970s until 1990, world events (political, economical, energetic and environmental) have brought about periodic resurgences of interest in non-fossil and renewable sources of energy. By mid-1990, international oil prices reduced, and, as conflicts have been resolved as well as economic changes accommodated, these initiatives were gradually reduced. Presently, the situation changed dramatically, oil prices are continuously raising, pollution problems are worse and global warming is threatening the whole planet. Thus, renewable energy supplies are of steadily increasing importance in all countries (da Silva, 2012, and Hodge, 2011). In Brazil, as the global crisis aggravates, initiatives towards the development of clean and renewable sources of energy are starting to take place again. In particular, water current or hydrokinetic submerged river turbines are now being considerate to be explored commercially by Eletronorte. Unlike conventional hydro and tidal barrage installations, water current turbines can generate electricity from natural flowing rivers or streams, with almost zero environmental impact, over a much wider range of sites than those available for conventional tidal power generation. These turbines generate power from the kinetic energy of a flowing stream of water without the use of a dam or barrage. Water current turbines can be installed in any flow with a velocity greater than 1.5 m/s (Asseff, 2009, Eggleston and Stoddard, 1987). Systems can be installed in isolated or grid connected configurations, stand alone or as a supplement to existing generators, floating or fixed to the bottom of a water course. Since many remote communities are situated near moving water these turbines represent a promising source of clean power. This work is mainly concerned with the development of a three-bladed rotor, horizontal axis, 10 m diameter, 500kW river current hydrokinetic turbine, planned to be installed downstream to Tucuruí Dam, in the state of Para, to generate electricity.

Hydrokinetic turbines are a class of “zero-head” hydropower and typically operate in flow regimes where the flow direction is more predictable than for wind turbines and hence yaw mechanisms can be simplified or eliminated. Hydrokinetic turbines operate on many of the same principles as wind turbines and share similar design philosophies. Meanwhile, wind turbines have grown in size over the past decades, using larger rotors and taller towers to take

ISSN 2176-5480

advantage of the faster winds aloft and to maximize the use of plant infrastructure (Yukio, et al., 2009). In contrast, hydrokinetic turbines are limited in size by the dimensions of the channel they are placed in. Passively controlled fixed-speed stall-regulated hydrokinetic turbines are unlikely to attain an annual energy production as high as actively controlled variable-speed variable-pitch turbines, which are common in the wind industry. However, fixed-speed stall-regulated rotors have the potential to be more reliable and less costly due to the absence of extra control mechanisms and fewer moving parts. Moreover, in environments that have less variability in flow conditions, such as rivers in comparison to tidal straits, the added complexity and cost of a variable-speed rotor and variable-pitch blades may not be economically justifiable.

The most notable difference in a water current turbine is that the density of water is about 850 times greater than air so the energy in a given flow stream is much greater for a hydrokinetic turbine than for a wind turbine. However, average flow velocities for a tidal or river flow tend to be an order of magnitude lower than flow velocities at a good wind site. The net impact is that the Reynolds numbers tend to be in the same range for both wind turbines and hydrokinetic turbines, which allows for much of the same experimental airfoil/hydrofoil data to be used in the design process. Additionally, hydrokinetic turbines can be analyzed and designed using the same incompressible flow techniques used for wind turbines.

This work is concerned with the development of solid and hollow (shell type) metallic blades for a passively controlled stall-regulated, horizontal axis, three blades hydrokinetic turbine. Its nominal diameter is 10 m and the aim of this study is to present the preliminary design, as well as the structural analysis of the blades. Initially, taking into account the hydrodynamic loads at 30 rpm, a static stress analysis of 4.25 m long blades, as showed in Figure 1, fully clamped at its root, manufactured either with Al-Mg-Si alloy (AA 6061-T6) or stainless steel, AISI-304, will be considered. The distance from the center of the turbine axis to the tip of the blade is 5.00 m. And, between the root of the blade and a hub, in the turbine axis, there is a transition segment, which appears only at Fig. 6.

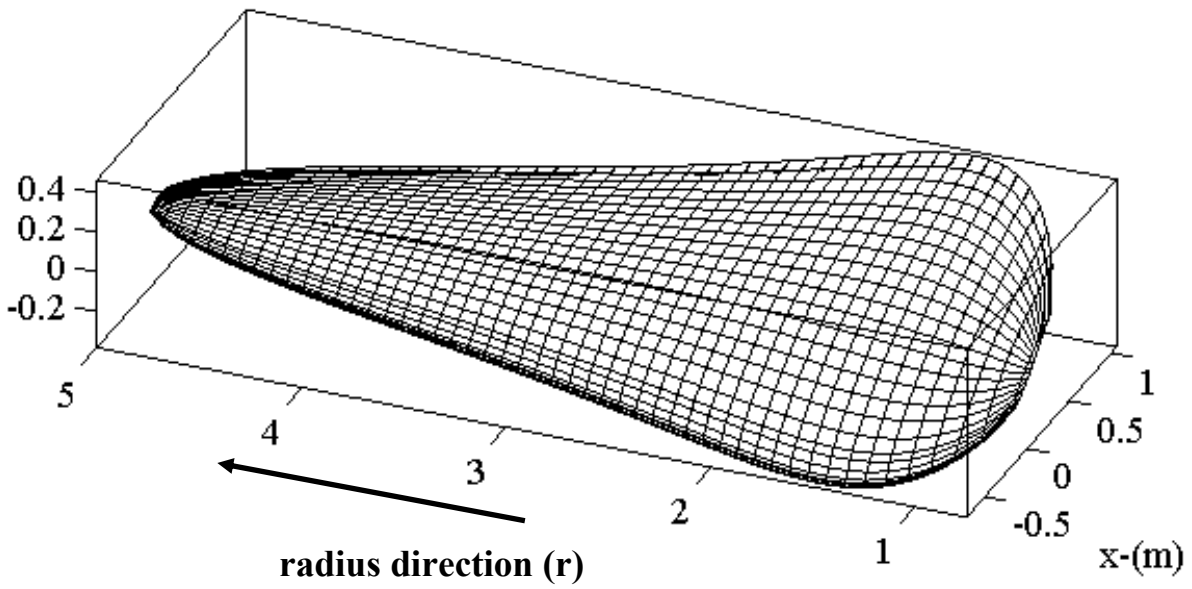

Figure 1. External geometry of the 5 m long blade under development (the right end is fully clamped).

2. METHODOLOGY AND DESIGN VARIABLES

2.1. Hydrodynamic loads

The simulated blades were developed from 50 hydrodynamic profiles obtained using a methodology based on the theory known as BEM (blade element momentum). As a result, from the application of this theory, the obtained profiles (NACA 65_3-618), which generate and define the external geometry of the blade, have continuous variable chord and angles of attack, according to Fig. 1. The turbine works immersed into the water and the river flow, perpendicular to the rotor plane, interact with the blades making them rotate. Thus, in order to calculate the stresses acting on them, taking as reference the vertical plane in which the blades rotate (i.e. the rotor plane), as shown in Figs. 2 and 3, the applied distributed loads on each blade were specified as normal (represented by vector F_n in Fig. 3) and tangential (see vector F_t in Fig. 3) to the rotor plane. These loads, measured in kN per meter (kN/m), are continuously distributed along the radius (r) of the blade, from the clamped base (which is connected to a hub, in the axis of the turbine, by means of a

ISSN 2176-5480

0.75 meters long transition segment, not shown in Fig. 1) towards the free end tip. The normal and tangential distributed loads, as well as the resultant of these distributed forces, are presented in Figs. 4 and 5. The resultant force acting on each blade is W = 55.3 kN (5637 Kgf). In Fig. 3, the vectors L and D represent the lift and drag forces, respectively, acting on the blade.

Figure 2. From and back views of the 3 blades floating turbine

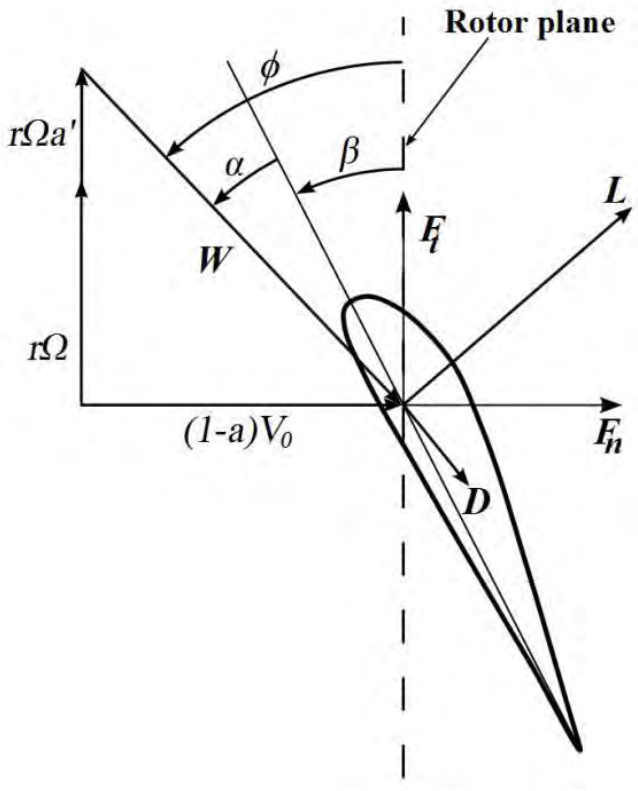

Figure 3. Representation of the aerodynamic loads relatively to the rotor plane

ISSN 2176-5480

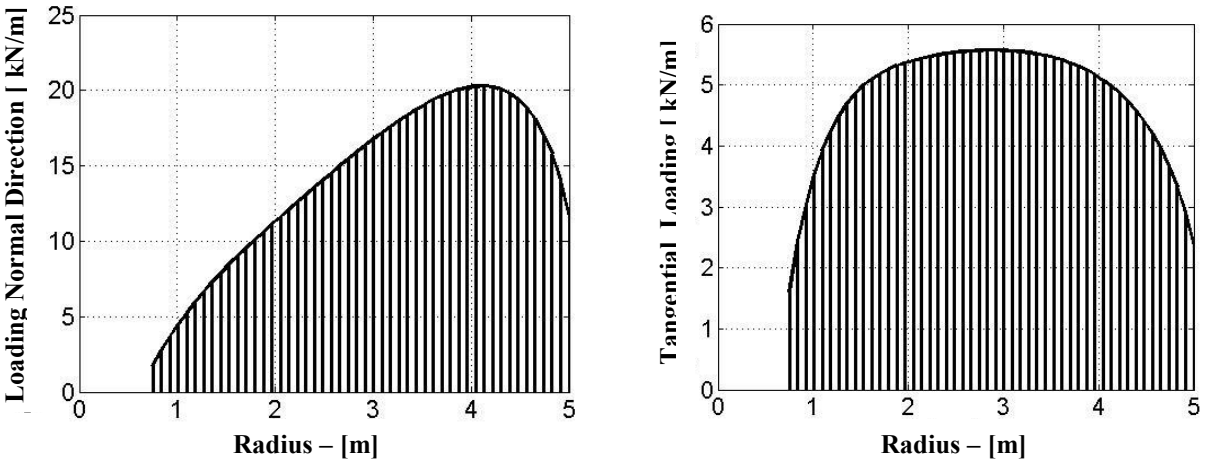

Figure 4. Normal, at left, and tangential, at rigth, distributed loads, relatively to the rotor plane.

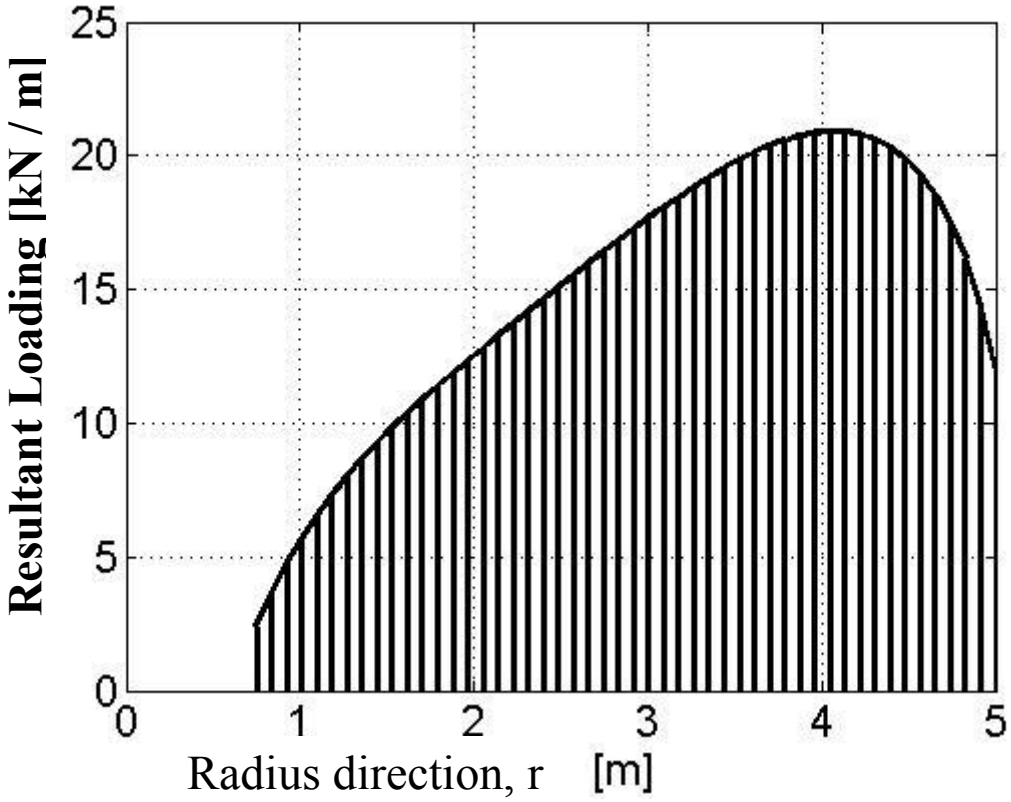

Figure 5. Resultant from the normal and tangential distributed loads (kN/m) acting in one blade

2.2 Finite element model

Adopting the geometry shown in Fig. 1, as well as the resultant distributed load presented in Fig. 5, static numerical models for each blade were created, using the finite element (FE) program ANSYS. The FE mesh was implemented using Ansys Mechanical APDL. In particular, varying the material and the architecture of the blades, four kinds of models were implemented: (i) solid blade, as presented in Fig. 6, made of aluminum alloy (AA 6061 T6 Al-Mg-Si); (ii) solid blade of stainless steel, AISI 304; (iii) AA 6061-T6 hollow blade (skins with a web and spars, as shown in Fig. 7); and (iv) AISI 304 hollow blade.

The model presented in Fig. 6 includes the 4.25 m long hydrodynamic blade (see Fig. 1) and a 0.50 m long transition segment. This segment starts at a hub, with a circular cross section, changes to an elliptical section and then is connected to the first hydrodynamic profile. As can be noticed in Fig. 7, the web is a circular tube (external diameter 200 mm and shell wall 20 mm). It is connected to a hub, in the turbine axis, and goes up to the radial coordinate r = 3

ISSN 2176-5480

m. A series of transversal spars, of thickness 20 mm, were connected to the web. Since the web is cylindrical, it is easy to adjust the spars to the attack angle of each hydrodynamic profile. The top and bottom skins, which are also 20 mm thick, are connected to spars to complete the hollow blade.

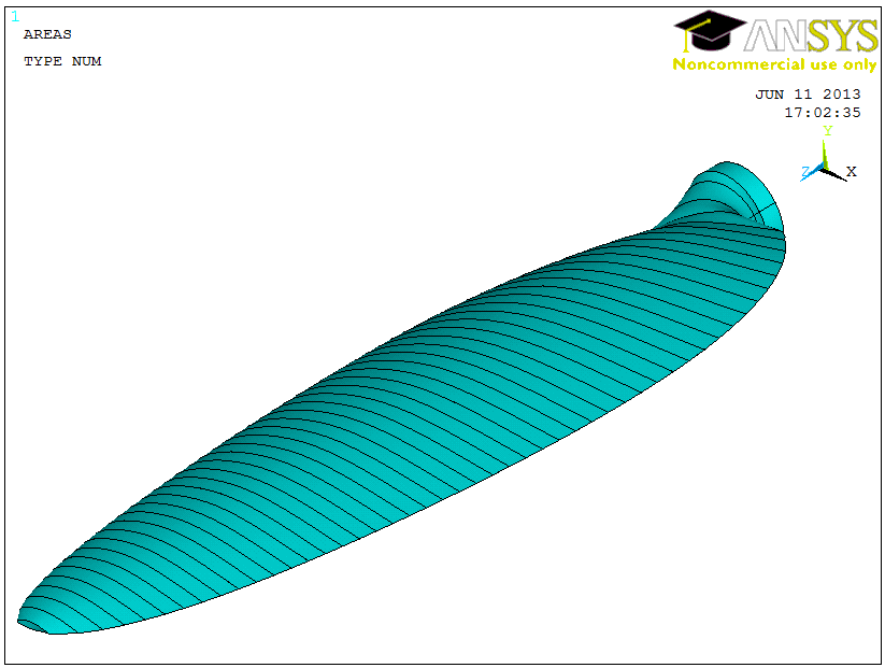

Figure 6. External geometry of the solid blade

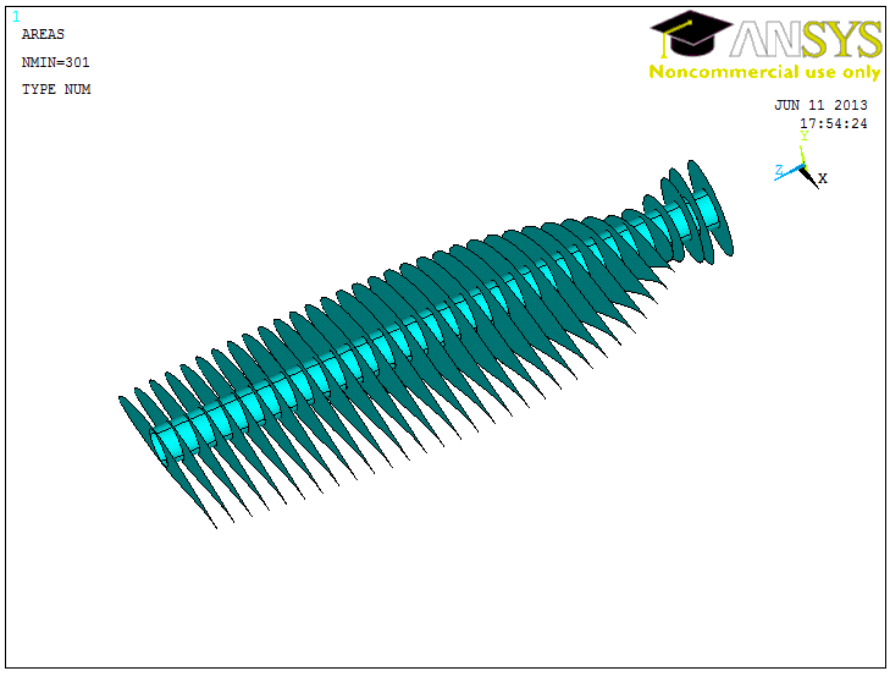

Figure 7. Web in direction z and spars in direction x of the hollow blade.

The meshes of the solid blades (I, Al) and (ii, steel), which converged with 59007 elements and 102750 nodes, were created using the 3-D ANSYS element solid 187. The mesh for the hollow blades, on the other hand, started with the creation of 50 hydrodynamic profiles, with 50 points each, totalizing 2500 points. The first and last point in each profile were coincident, closing a loop of 49 points. Each point, with its respective coordinates, was converted into a keypoint. For each profile were created 2 splines, one for the top skin and another for the bottom skin, which meet at poins 1 and 25. The profiles were connected with guide lines along the meeting points (poins 1 and 25, of each profile), at the leading and trailing edges of the blade, forming a skeleton. A representation of the skeleton, after 36 profiles were

ISSN 2176-5480

created and connected, is shown in Fig. 8. After the skeleton with the 50 connected profiles was complete, 100 areas were created. Finally 50 areas were condensated into the top skin and the other 50 into the bottom skin.

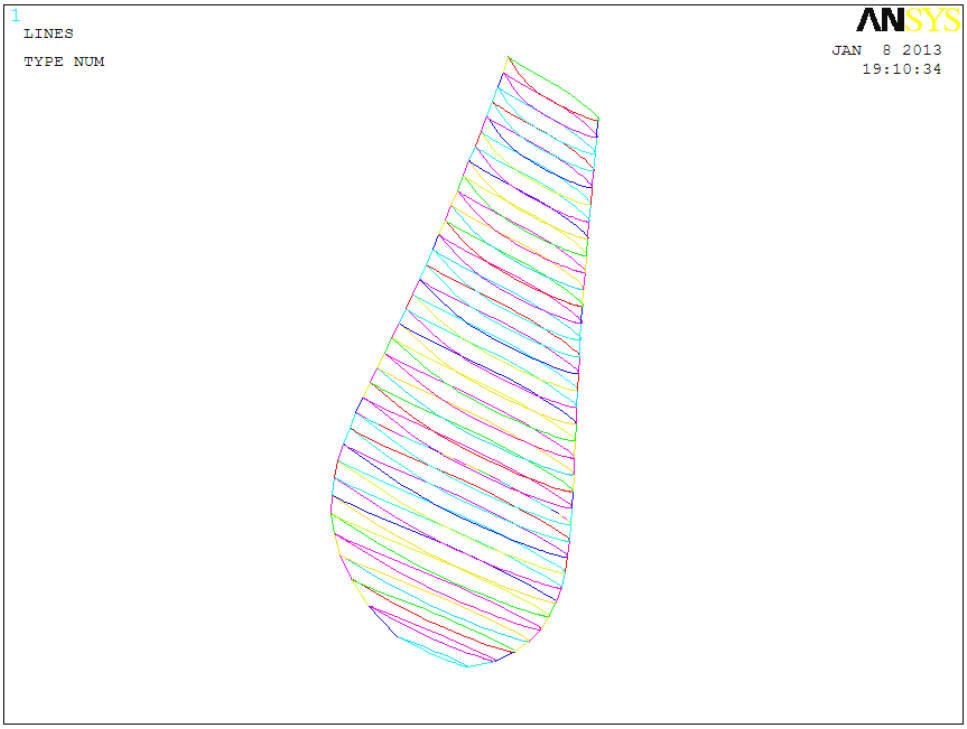

Figure 8. Skeleton with pairs of splines and guide lines for the first 36 profiles

2.3. Mechanical properties of materials

Four models were created: two solid blades (see Fig. 6), made of (i) aluminum 6061-T6, and (ii) stainless steel 304; as well as two shell type blades (with skins, web and spars, see Fig. 7), made of (iii) aluminum 6061-T6, and (iv) stainless steel 304. The mechanical properties of aged aluminum 6061-T6 and annealed stainless steel AISI 304 are presented in Tab. 1.

Table 1.Mechanical Properties of the Metallic Alloys (Callister Jr., 2007)

Properties	AA6061-T6 (aged)	AISI 304 (annealed)
Yield stress (σ_y), MPa	276	205
Ultimate stress (σ_u), MPa	310	515
Fatigue limit (σ_f), MPa	96.5	170
Rupture strain, %	17	40
Elasticity Modulus (E), GPa	68.9	193
Poisson ratio (ν)	0.33	0.30
Density (ρ), g/cm^3	2.7	8.0

3. MAIN RESULTS

Based on the numerical simulations carried out so far, the equivalent Von Mises stresses as well as the vertical deflections were obtained. In all ANSYS models the blades were fully clamped at the root, r = 0, the distributed loads started at r = 0.75 m, the centrifugal loads due to the angular rotation (30 rpm) were combined with the distributed hydrodynamic forces, and coordinate z was coincident with the radial direction z (i.e. z ≡ r). The Von Mises stresses, σ_{VM}, as well as vertical deflections, δ_y, are presented in Figs. 9 to 12. The maximum tensile and compressive stresses along the radial direction $\sigma_z = \sigma_r$ were also obtained. The numerical results for σ_z, σ_{VM} and δ_y are presented in Tab. 2.

ISSN 2176-5480

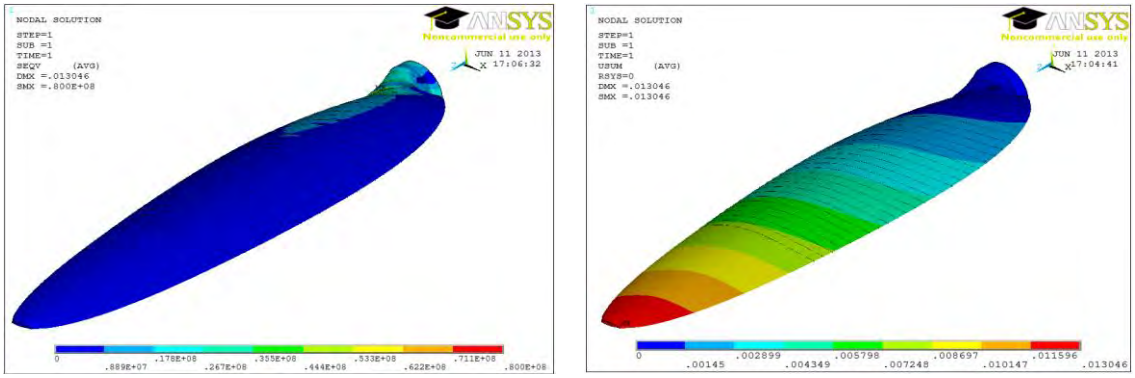

Figure 9. Von Mises stress (σ_{VM}, left) and vertical deflections (δ_y, right) distributions for the **hollow Al** blade

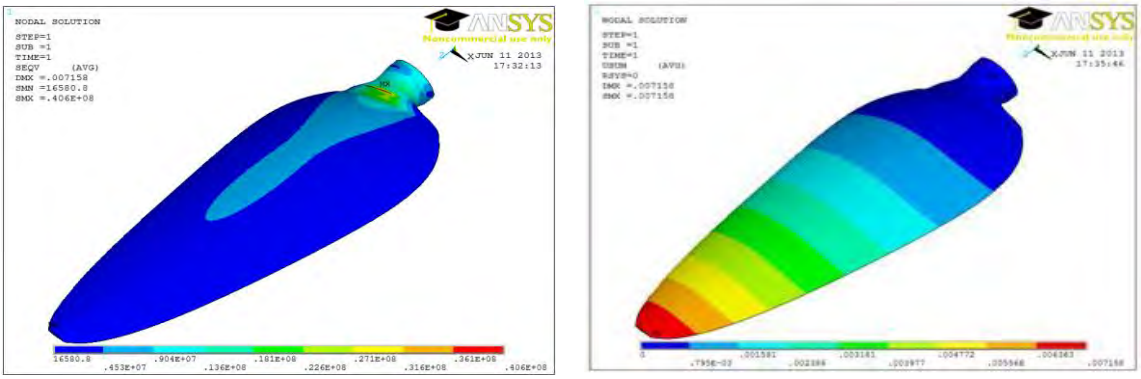

Figure 10. Von Mises stress (σ_{VM}, left) and vertical deflections (δ_y, right) distributions for the **solid Al** blade

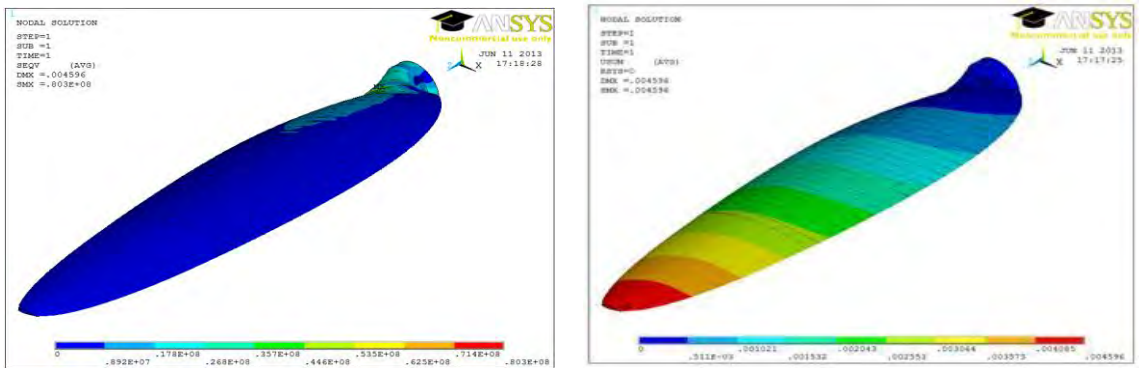

Figure 11. Von Mises stress (σ_{VM}, left) and vertical deflections (δ_y, right) distributions for the **hollow 304 steel** blade

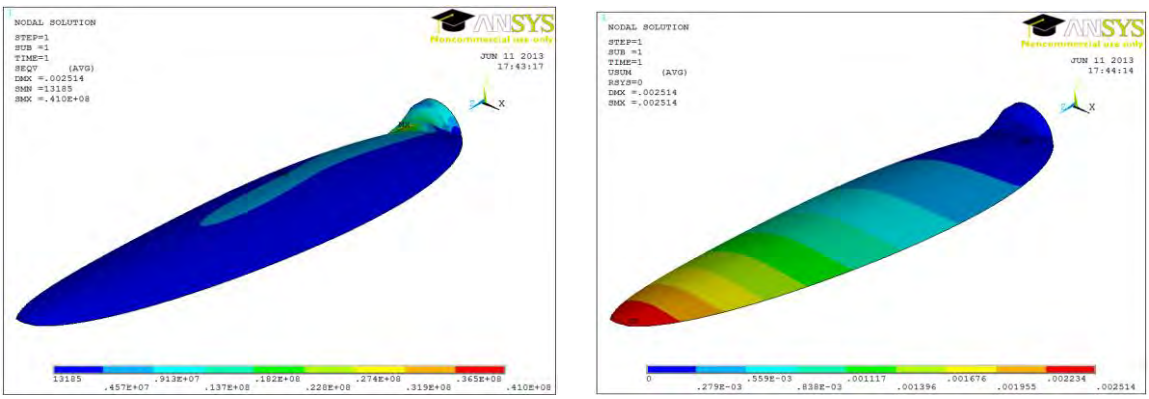

Figure 12. Von Mises stress (σ_{VM}, left) and vertical deflections (δ_y, right) distributions for the **solid 304 steel** blade

ISSN 2176-5480

None of the stresses shown at Figs. 9 to 12, in any region of the blades, reached the limit values concerned with the mechanical strength of the materials for yielding, rupture and fatigue. However, for the hollow blade of stainless steel, the maximum tensile stress reached about 70% of the fatigue limit. This is the major concern of the present work. In addition, the solid blades, which presented the lower stresses, are too heavy. The weight of the solid Al blade is 2575 Kgf and, for the solid steel blade 7630 Kgf.

4. ANALYSIS AND DISCUSSION OF THE RESULTS

A synthesis of the maximum numerical results obtained from the ANSYS simulations, including stresses and the vertical deflections at the tip of the blades (δ_y), is presented in Tab. 2. For the hollow (shell type) and solid blades, the obtained maximum Von Mises stresses (σ_{VM}), as well as the normal longitudinal tensile stresses due to bending (σ_z), can be directly analyzed and compared with yield (σ_y) and ultimate (σ_u) stresses of the materials (Al and stainless steel from Tab. 1), respectively. The maximum longitudinal tensile stress, σ_z , was also compared to the fatigue limit stress, σ_{FL} , and the deflection at the tip of the blades, δ_y, with the nominal length of the blades, L = 5000 mm.

Table 2. Comparison of ANSYS numerical results with the allowable stresses of the materials for each blade and maximum vertical deflections (δ_y)

Results / Ratios	**Al 6016-T6 hollow blade**	**Al 6061-T6 solid blade**	**Steel AISI 304 hollow blade**	**Steel AISI 304 solid blades**
Maximum σ_{VM} MPa	80.0	40.6	80.3	41.0
Maximum σ_z MPa	67.5	29.9	67.5	29.9
Maximum δ_y mm	13.046	7.158	4.596	2.514
Maximum (σ_{VM} /σ_y)	0.290	0.147	**0.392**	0.200
Maximum (σ_z /σ_u)	**0.218**	0.096	0.131	0.058
Maximum (σ_z /σ_{FL})	**0.699**	0.310	0.397	0.176
Max. **100**.(δ_z /L)	**0.26 %**	0.14%	0.092%	0.050%

The combination of the ANSYS results with the mechanical properties of the materials, as well as the nominal length of the blades, provided some ratios that estimates how far are the blades to present: a - plastic deformations; b – catastrophic fracture; c - fatigue failure; and d - to deflect too much.

a - For the onset of **plastic deformation**, the most critical blade (i.e. with the lowest safety factor) was the **hollow blade of stainless steel**, in which the Von Mises stress reached **39.2%** of the yield stress. The reason for that is the fact that the yield stress of the annealed stainless steel 304 is lower than that of Al 6061-T6 (aged). However, even for this blade, the safety factor for the onset of plastic failure is higher than 2. In addition, if the stainless steel is subjected to cold work, then its yield stress can be higher than that of Al 6061-T6.

b – As far as catastrophic **fracture** is concerned, the most critical blade (i.e. with the lowest safety factor) was the **hollow blade of Al 6061-T6**, in which the ultimate tensile stress reached **21.8%** of the yield stress. However, even for this blade, the safety factor for rupture is higher than 4.

c – As far as **fatigue failure** is concerned, the most critical blade (i.e. with the lowest safety factor) was the **hollow blade of Al 6061-T6**, in which the ultimate tensile stress reached **69.9%** of the fatigue limit stress.

d – As far as **deflection** is concerned, the most critical blade (i.e. with the lowest safety factor) was the **hollow blade of Al 6061-T6**, in which the tip deflection stress reached **0.26%** of the nominal length of the blade. However, this value is well accepted for practical situations (Eggleston and Stoddard, and Abbot and Doenhoff, 1959).

For both types of blades, the highest Von Mises stresses occurred at to root of blades, very close to the clamped edges. For the hollow blades, the region with the higher stresses was relatively more localized.

5. CONCLUSIONS

None of the stresses shown at Figs. 9 to 12, in any region of the blades, reached the limit values concerned with the mechanical strength of the materials for yielding, rupture and fatigue, presented in Tab. 2.

The maximum equivalent Von Mises stress (close to the clamped root) is less than 40 % of the yield stress of the alloys, in the worst case (hollow shell type stainless steel AISI 304 blade). Thus, as far as plastic failure is concerned, there is a safety factor greater than 2 for the most critical blade.

ISSN 2176-5480

The maximum tensile stress reached about 70% of the fatigue limit stress of the aluminum 6061-T6, in the worst case (hollow shell type Al blade). Presently, this is the major concern for the development of the hydrokinetic turbine blades. Thus, since the safety factor for fatigue failure is less than 1/3, the next step of the work is the optimization of the design. In particular, to reinforce the blades in the region close to the clamped root.

6. 6. ACKNOWLEDGEMENTS

The authors are grateful for the support they received from CNPq, Petrobrás and Eletronorte.

7. REFERENCES

Abbot, J.H. and Doenhoff, V., 1959, “Theory of Wing Sections”. Dover Publications Inc, 2nd edition.

Asseff, N.S., 2009. “Design and finite element analysis of an ocean current turbine blade”. Ph.D. thesis, Florida Atlantic University, Dania Beach.

Callister Jr., W.D., 2007. “Ciência e Engenharia dos Materiais - uma introdução”, LTC, Rio de Janeiro.

Eggleston, D. M. and Stoddard, F. S, 1987. “Wind Turbine Engineering Design”. Van Nostran Reinhold, New York.

Hodge B. K., 2011, “Sistemas e Aplicações de Energia Altenativa”. LTC, Rio de Janeiro.

Yukio, I., Tsuyoshi, I. and Kohei, N., 2009. “Vibration of a Wind Turbine Blade: Theoretical Analysis and Experiment Using a Single Rigid Blade Model. Journal of Environmental and Engineering. Vol. 4(20), pp. 443-454.

da Silva, C.G., 2012. “De Sol a Sol, energia no século XXI”. Oficina de Textos, São Paulo.

8. RESPONSIBILITY NOTICE

The authors are the only responsible for the printed material included in this paper.